Perovskite Catalysts

DOI: 10.1002/ange.201311223

A Bifunctional Perovskite Catalyst for Oxygen Reduction and Evolution**

Jae-Il Jung, Hu Young Jeong, Jang-Soo Lee, Min Gyu Kim, and Jaephil Cho**

Abstract: *$La_{0.3}(Ba_{0.5}Sr_{0.5})_{0.7}Co_{0.8}Fe_{0.2}O_{3-\delta}$ is a promising bifunctional perovskite catalyst for the oxygen reduction reaction and the oxygen evolution reaction. This catalyst has circa 10 nm-scale rhombohedral $LaCoO_3$ cobaltite particles distributed on the surface. The dynamic microstructure phenomena are attributed to the charge imbalance from the replacement of A-site cations with La^{3+} and local stress on Co-site sub-lattice with the cubic perovskite structure.*

Much of the-state-of-the-art catalysis research is focused on developing non-precious metal-based catalysts that can perform well enough to replace precious and scarce metal-based catalysts.[1] Among noble-metal-free alternatives, the perovskite-based catalysts provide advantage over precious metal-based catalysts from the aspect of low price, high endurance at high temperature, and less weight during application.[2] Recently, $Ba_{0.5}Sr_{0.5}Co_{0.8}Fe_{0.2}O_{3-\delta}$ (BSCF5582)-based complex perovskite oxide is being spotlighted as a competitive candidate of bifunctional catalyst in the oxygen reduction reaction (ORR) and oxygen evolution reaction (OER) catalysis.[3] As a mixed electronic and ionic conductor, BSCF5582 exhibits fast oxygen exchange kinetics and ionic conductivity, facilitating the movement of oxygen anions through oxygen vacancies, which enables it to be proper for such diverse applications as oxygen membranes and intermediation temperature solid oxide fuel cell (IT-SOFC) cathode materials.[4]

Shao-Horn et al. reported that any transition-metal oxide perovskite, which has an e_g-filling (σ^*-orbital occupation) close to 1, shows the maximum ORR activity, on the base that the B-site transition-metal–oxygen covalency between metal-3d and oxygen-2p works as a criterion in determining catalytic activity.[3] Even in designing OER catalysts, the $Ba_{0.5}Sr_{0.5}Co_{0.8}Fe_{0.2}O_{3-\delta}$ (BSCF5582) that has $e_g \approx 1.2$ with $t_{2g}^5 e_g^{\approx 1.2}$ in the electronic configuration of Co cations exhibits the highest OER activity among perovskite oxide candidates, the performance of which is nearly identical to IrO_2 at a catalytic activity.[3] This shows that any complex perovskite oxide based on BSCF can be a strong candidate of bifunctional catalyst in the variable oxygen electrochemical applications, such as metal–air batteries and fuel cells. The novel architecture of complex perovskite oxides by monitoring the types and distributions of defects within phase structure can contribute to upgrading the electrochemical performance of ceramic-based catalysts. Dynamic alteration of cations and oxygen non-stoichiometry by chemical substitution is useful in mediating the stability, crystal structure, and functionality of perovskite oxide systems.

Herein, we introduce a novel bifunctional catalyst based upon BSCF5582 peroviskte oxide, which is distributed with $LaCoO_{3-\delta}$ cobaltite particles on the surface. The catalytic performance of the newly introduced catalysts is discussed in comparison with precious metal-based catalysts, where the obtained electron transfer number (n) in ORR activities of $La_{0.3}(Ba_{0.5}Sr_{0.5})_{0.7}Co_{0.8}Fe_{0.2}O_{3-\delta}$ ($La_{0.3}$-5582) is 3.60–3.72, while RuO_2 and BSCF5582 show 3.63–3.77 and 3.20–3.26, respectively, and the OER activity of $La_{0.3}$-5582 was 2–3 times higher than that of BSCF5582, exhibiting $La_{0.3}$-5582as a promising bifunctional electrocatalyst (Figure 1a). Compared with the conventional powder morphology of BSCF5582 with a round shape, $La_{0.3}$-5582 is shaped as flowerly particles, with the average particle sizes of BSCF5582 and $La_{0.3}$-5582 as 10.4 ± 6.3 μm and 1.8 ± 1.3 μm, respectively (Figure 1a; Supporting Information, Figure S1). Furthermore, circa 10 nm-size rhombohedral $LaCoO_{3-\delta}$ particles are distributed at random on the grain surface of $La_{0.3}$-5582 particles (Figure 1a), the element composition of which was analyzed by TEM EDS (Supporting Information, Figure S3d and Table S1). The pseudo-cubic peaks in $La_{0.3}$-5582, which are located at higher angles than those of BSCF5582, with the lattice constants of 3.89 Å and 3.98 Å, respectively, are observed more obviously at $\geq 2\theta = 50°$ in X-ray diffraction patterns (Supporting Information, Figure S2). This implies that the complex perovskite cubic structure, while undergoing buckling and rearrangement with the addition of a higher valence of A-site cation (La^{3+}) to BSCF5582, is impregnated with different symmetry of structures (Figure 1; Supporting Information, Figure S2).

The cross-sectional high-angle annular dark field (HAADF) STEM images prepared by focused ion beam (FIB) show that circa 10 nm size of secondary nanoparticles

[*] Dr. J. Jung, J. Lee, Prof. Dr. J. Cho
School of Energy and Chemical Engineering
Ulsan National Institute of Science & Technology (UNIST)
Ulsan 689-798 (South Korea)
E-mail: jpcho@unist.ac.kr
Homepage: http://jpcho.com
Dr. H. Jeong
UNIST Central Research Facilities (UCRF)
Ulsan National Institute of Science & Technology (UNIST)
Ulsan 689-798 (South Korea)
Dr. M. Kim
Beamline Research Division, Pohang Accelerator Laboratory,
Pohang University of Science and Technology
Pohang 790-784 (South Korea)
E-mail: mgkim@postech.ac.kr

[**] This work was supported by the next generation battery R&D program of MOTIE/KEIT (10042575) and the BK21 Plus funded by the Ministry of Education, Korea (10Z20130011057).

Supporting information for this article is available on the WWW under http://dx.doi.org/10.1002/anie.201311223.

 © 2014 Wiley-VCH Verlag GmbH & Co. KGaA, Weinheim

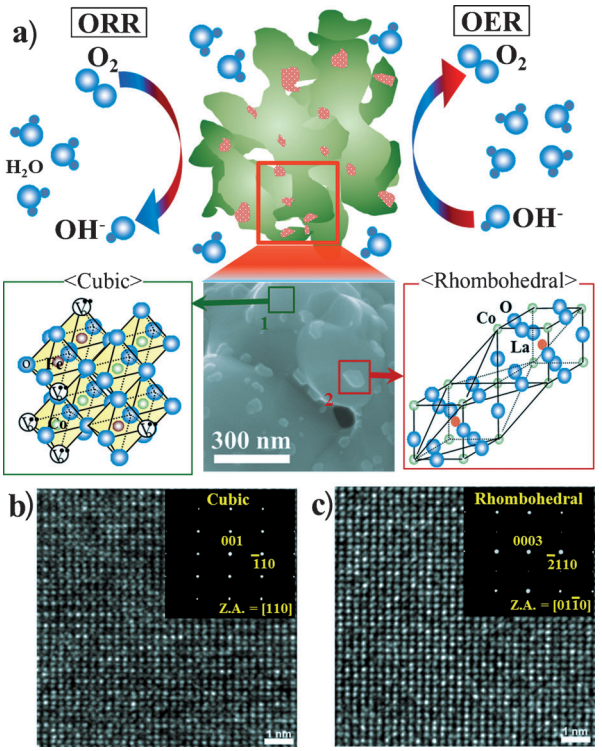

Figure 1. a) A representation of the bifunctional catalytic performance of the perovskite catalyst $La_{0.3}(Ba_{0.5}Sr_{0.5})_{0.7}Co_{0.8}Fe_{0.2}O_{3-\delta}$ ($La_{0.3}$-5582). On the surface of cubic based grains, the rhombohedral phase $LaCoO_{3-\delta}$ grains are segregated. a), b) HRTEM images and corresponding SAED patterns of (b) region 1 and (c) region 2 in rectangular areas in the SEM image.

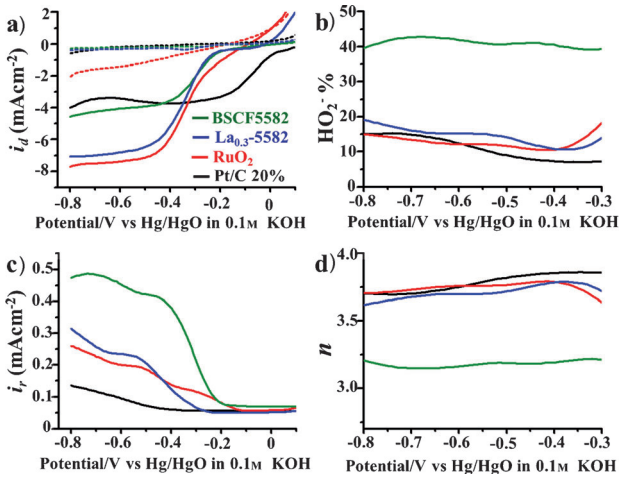

Figure 2. Electrocatalytic properties (ORR) of 80 wt% $Ba_{0.5}Sr_{0.5}Co_{0.8}Fe_{0.2}O_{3-\delta}$ on 20 wt% Ketjenblack(KB) composite (BSCF5582), 80 wt% $La_{0.3}(Ba_{0.5}Sr_{0.5})_{0.7}Co_{0.8}Fe_{0.2}O_{3-\delta}$ on 20 wt% KB composite ($La_{0.3}$-5582), and 80 wt% RuO_2 on 20 wt% KB composite-(RuO_2). a) disc and c) ring currents of the ORR using RRDEs at 1600 rpm and 10 mVs^{-1} scan rate in 0.1 M KOH under the saturated oxygen gas (line) and under the saturated argon gas (dot). $La_{0.3}$-5582 (blue), BSCF5582 (green), RuO_2 (red), and 20wt% Pt on Vulcan XC-72 composite (E-tek) (Pt/C 20%) (black), where the loading amounts of materials are 0.639 $mg_{ox}\,cm^{-2}$ and 0.157 $mg_{pt}\,cm^{-2}$ for oxide materials and Pt, respectively, and the determined b) peroxide percentage (HO_2^-%) and d) electron transfer number (n).

are randomly distributed on the surface of the grains in $La_{0.3}$-5582, in contrast with the simple surface of BSCF5582 grains (Supporting Information, Figure S3a,b). The EDS spectra obtained at region 2 of Figure S3b confirm that the aggregates are mainly composed of La, Co and O elements (Supporting Information, Figure S3c,d, Table S1). The selective area electron diffraction (SAED) pattern and HRTEM image reveal that the structure of aggregate is a rhobohedral aligned with [01−10] electron beam direction, showing a (0003) weak spot. In consideration with the overall XRD, HRTEM and EDS analyses, we concluded that the formed secondary nanoparticles on the surface of $La_{0.3}$-5582 are the rhombohedral structure $LaCoO_{3-\delta}$. The space group of rhombohedral $LaCoO_{3-\delta}$ has $R\bar{3}c$ symmetry, exhibiting a rhombohedrally distorted ABO_3 perovskite with unequal Co−O bond lengths. The structural distortion is attibutable to a JT distortion and implies the long-range ordering of the e_g orbitals, where p and d orbitals are spatially overlapped and the electrons interact by exchange on adjacent lattice ions.[5] With the differentiation of Co−O bond lengths, La^{3+} cations displace in that ⟨111⟩ directions, which will cause the cubic perovskite structure to be locally distorted into a rhombohedrally distorted ABO_3 perovskite structure (Figure 1a).

The ORR activities of BSCF5582 and $La_{0.3}$-5582 composite electrode consisting of 80 wt% sample and 20 wt% Ketjenblack (KB600) were investigated using rotational ring-disk electrodes (RRDEs). Figure 2a shows the typical voltammograms at a potential scanning rate of 10 mVs^{-1}. The disk currents reflect the catalytic ORR on the base of the negligible cathodic currents in an Ar-saturated electrolyte. The average particle sizes of RuO_2 and KB are 60 ± 15 nm and 20 ± 5 nm, respectively (Supporting Information, Figure S4a,c). The linear sweep voltammograms show that the onset potentials of BSCF5582, $La_{0.3}$-5582, and RuO_2 are quite similar at −0.25 V, which is comparable with that of Pt/C 20%, 0 V (Figure 2a,b). The limiting currents of the $La_{0.3}$-5582 and RuO_2 are −7.0 mA cm^{-2} and −7.5 mA cm^{-2}, respectively, which are significantly higher than those of Pt/C 20% and BSCF5582, both of which are close to −4 mA cm^{-2}. There is a significant enhancement of ORR catalytic activity in BSCF-based perovskite oxide, which approaches to the performance of RuO_2, as 0.3 mol% of La_2O_3 is doped to BSCF5582 in the placement of A-site cations, Ba and Sr. At a given specific current within the half-wave potential range between −0.25 and −0.43 V, the potential of $La_{0.3}$-5582 is quite similar to that of RuO_2, with a slight difference of 20–40 mV. Intrinsically, there is a great peroxide yield in BSCF5582, which is denoted by the high ring current of BSCF5582, that is twice that of both $La_{0.3}$-5582 and RuO_2 (Figure 2c). The ORR catalytic performance can also be evaluated with the calculated electron transfer number (n) and peroxide yield (HO_2^-%) that come from disc (i_d) and ring (i_r) currents. Over the potential range of −0.8 and −0.3 V, the obtained n of $La_{0.3}$-5582 is 3.60–3.72, which shows approximately close to those of RuO_2 and Pt/C 20% with 3.63–3.77 and 3.70–3.80, respectively, whilst n of BSCF5582 is 3.20–3.26. This suggests that $4e^-$ reduction is dominant in the ORR activity of $La_{0.3}$-5582, with higher n and lower HO_2^-% than

 © 2014 Wiley-VCH Verlag GmbH & Co. KGaA, Weinheim

BSCF 5582. The competitive electrochemical performance of La-doped BSCF complex perovskite oxide could be attributable to the increased active sites, according to surface area increase, which in turn can be explained as the optimized microstructure suitable for ORR catalytic activity (Supporting Information, Figures S5–S7). Besides the promising performance of ORR activity, $La_{0.3}$-5582 demonstrates an outstanding catalytic durability with a consistent and linear decrease up to 82% of relative current (i/i_o) until 30000 s without any serious hunting, which is quite comparable with the performance of RuO_2 that decreased up to 85% of i/i_o until 30000 s (Figure 3b).

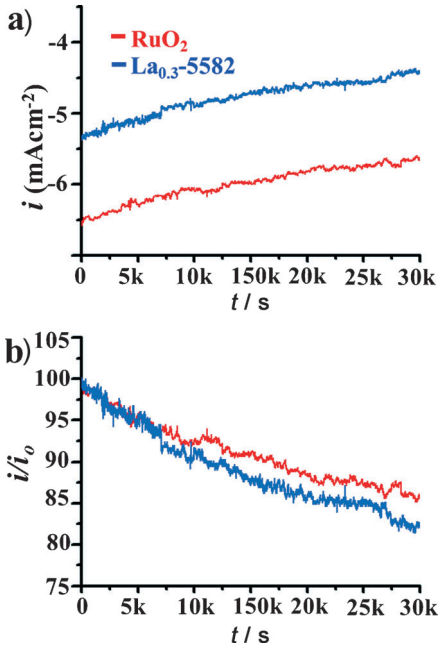

Figure 3. Electrocatalytic properties (Chronoamperometric methods) of a) disc (i) and b) relative (i/i_o) currents using RDEs at 1600 rpm and −0.6 V of a fixed potential in 0.1 M KOH under the saturated oxygen gas. 80 wt% $La_{0.3}(Ba_{0.5}Sr_{0.5})_{0.7}Co_{0.8}Fe_{0.2}O_{3-\delta}$ on 20 wt% KB composite ($La_{0.3}$-5582) and 80 wt% RuO_2 on 20wt% KB composite (RuO_2), where the loading amount of materials is 0.639 $mg_{ox}\,cm^{-2}$.

Shao-Horn et al. recently introduced BSCF5582 as the highly active OER catalyst with the electronic configuration of Co cations assigned as $t_{2g}^{5}e_g^{\approx 1.2}$, more than one order higher OER activity than IrO_2 (ca. 5 μm, Sigma–Aldrich 99.9%; Supporting Information, Figure S4b).[3] In the same way, our result shows that the OER activity of BSCF5582 is nearly one order higher than the commercial IrO_2 (Figure 4). Furthermore, the OER activity of $La_{0.3}$-5582 is 2–3 times higher than that of BSCF5582. This outstanding catalytic performance both in ORR and OER indicates that the La-doped BSCF complex perovskite oxide can be counted as the promising bifunctional catalyst in the next generation (Figure 4), where it is noteworthy that the La-doped BSCF complex perovskite oxide ($La_{0.3}$-5582) introduced in this study 1) has almost ten times smaller particle size than that of BSCF5582 (Supporting Information, Figure S1), and 2) keeps rhombohedral

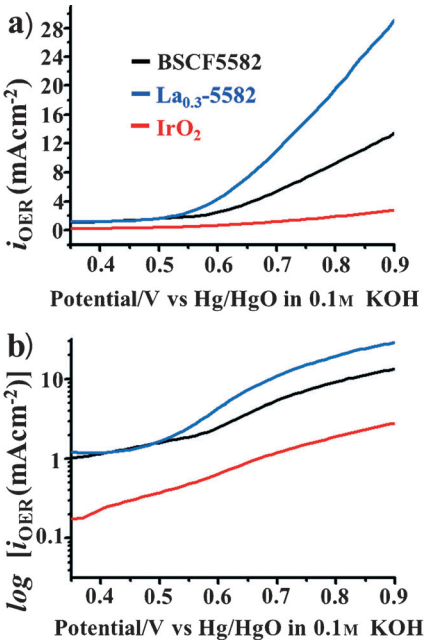

Figure 4. a) Linear and b) logarithmic scale of OER activities of 80 wt% $Ba_{0.5}Sr_{0.5}Co_{0.8}Fe_{0.2}O_{3-\delta}$ on 20 wt% Ketjenblack (KB) composite (BSCF5582), 80 wt% $La_{0.3}(Ba_{0.5}Sr_{0.5})_{0.7}Co_{0.8}Fe_{0.2}O_{3-\delta}$ on 20 wt% KB composite ($La_{0.3}$-5582) and 80 wt% IrO_2 on 20 wt% KB composite (IrO_2), where the loading amount of materials is 0.639 $mg_{ox}\,cm^{-2}$. BSCF5582 (black line), $La_{0.3}$-5582 (blue line), and IrO_2 (red line) as a function of potential on GCE in oxygen saturated 0.1 M KOH electrolyte at 10 $mV\,S^{-1}$ scan rate at 1600 rpm.

$LaCoO_{3-\delta}$ aggregates as a secondary phase (Figure 1, Supporting Information, Figures S2 and S3), which are expected to contribute synergically to the performance of electrocatalysis.

As La_2O_3 is doped to BSCF5582 ($Ba_{0.5}Sr_{0.5}Co_{0.8}Fe_{0.2}O_{3-\delta}$), La^{3+} is expected to occupy the regular A-site cation (Ba^{2+}, Sr^{2+}) lattice sites, $La_A^{\bullet}$, as shown in Equation (1):

$$La_2O_3 \xrightarrow{AO} 2La_A^{\bullet} + 2O_O + {}^1/_2O_2(g) + 2e^- \qquad (1)$$

The dissolved lanthanum ion is another type of defect with positive effective charge within the p-conductor oxide, and the empty oxygen site (oxygen vacancy) is occupied by the oxygen anion into O_O. The La-doping effect on the lattice structure was systematically investigated by analyzing the atomic-selective XAFS spectra of each atomic-edge for the perovskites BSCF5582 and $La_{0.3}$-5582 (Figure 5). Compared with the Fe K-edge spectra, the peak intensity ratio between pre-edge feature (peak A, 1s electron to 3d transition) and main absorption peak (peak B, 1s to 4p transition) in the Co K-edge XANES spectra increased significantly, and the edge inflection positions shifted towards the higher energy region as well (Figure 5a). It signifies that La-doping to BSCF5582 affected preferentially on the local structure of Co-sublattice octahedron, and the overall Co-sublattice octahedron become more centrosymmetric according to the peak feature at the Co K-edge of $La_{0.3}$-5582, while both Fe and Co cations are simultaneously oxidized (Figure 5). According to the radial distribution function (RDF) of EXAFS (Figure 5b), the

© 2014 Wiley-VCH Verlag GmbH & Co. KGaA, Weinheim

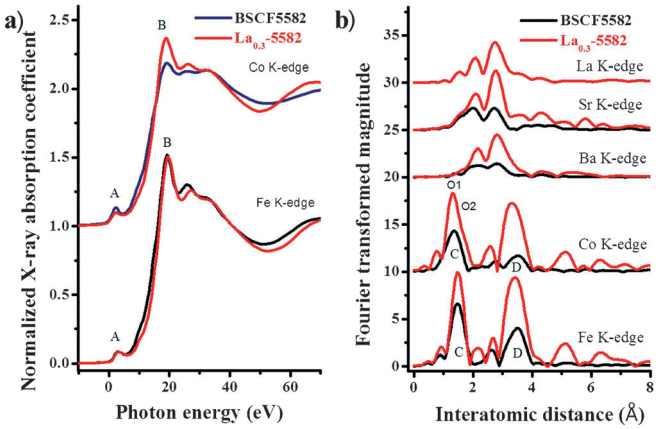

Figure 5. a) Normalized Fe and Co K-edge XANES spectra and b) radial distribution function for the all atomic EXAFS spectra for BSCF5582 and $La_{0.3}$-5582. The Fe and Co XANES spectra have been plotted with respect to each absorption edge-energy (Fe = 7112 eV and Co = 7709 eV).

Fourier-transformed (FT) peak intensities of $La_{0.3}$-5582 are shown to have increased greatly over the FT peak intensities of BSCF5582 in the all atomic edges, which means that the La-doping introduces the oxygen into the oxygen-vacant site of BSCF and promotes the stretch-up of the overall atomic arrangement in the perovskite lattice, where the first FT peaks correspond to a B–O bond and the third FT peaks to corner-shared B-O-B in the Fe- and Co-sublattice octahedrons of the three-dimensional perovskite structure. Moreover, the first FT peak of the Co K-edge is split into two FT peaks with lower and higher **r** spaces, while that of the Fe K-edge increased simply with constant **r** space, which implies the separation of Co–O bond into lower Co–O_1 and higher Co–O_2 bonds, which coincides with the argument of TEM analysis (Figure 1; Supporting Information, Figure S8a). Therefore, it is reasonable to argue that the selective impact of the La-doping can cause local stress on the unit cell of Co sub-lattice in cubic perovskite structure, while the unit cell of Fe-site sub-lattice remains less affected, giving rise to both the comminution of particles into smaller ones and the occurrence of rhombohedral $LaCoO_{3-\delta}$ aggregates simultaneously (Figure 1; Supporting Information, Figure S2).

On the assumption that defects are single, unassociated and randomly distributed within the ideal dilute solution model of lower defect concentration than 1 %, $x < 0.01$,[6] the overall electroneutrality condition is then described as Equation (2):

$$[B'_B] = [La_A^{\cdot}] + 2[V_O^{\cdot\cdot}] \quad (2)$$

In reality, in this study, with the addition of $La_A^{\cdot}$ to BSCF5582, the concentration of $V_O^{\cdot\cdot}$ decreases, while B-site cations of the B-site sub-lattices are rather oxidized and approach to B^{4+} without contributing to the product of B'_B. Some portions of Co cations, without being oxidized, are associated with $La_A^{\cdot}$ and contribute to the formation of a new defect structure, $LaCoO_{3-\delta}$ aggregates, in which the charge imbalance from the replacement of A-site cations with La^{3+} is generally understood as the main driving forces for structural ordering in the complex perovskite structure materials[7] and/or the selective structural stress on a B-site (Co-site) sub-lattice octahedron, as observed in this study.

The effect of the chemical oxygenation on the cubic perovskite unit cell is also clearly seen in the XPS spectra of O_{1s}, Ba_{4d}, Co_{2p3}/Ba_{3d5} (Supporting Information, Figure S9). On the base that oxygen anion exists as O^{2-} in the ⟨100⟩ direction of B-O–B bonds, the significant distribution shift from O^{2-} to O_2^{2-}/O^- implies that the typical cubic perovskite underwent a significant structure transformation through the chemical oxygenation.[8] The peak 781.5 eV, above 780 eV in Co_{2p3}/Ba_{3d5} peaks, implies that some portions of Co cations also exist as Co^{+4} in $La_{0.3}$-5582, which can be explained by the differentiated Co–O bond lengths and the structural stress loaded on the bonds of A-O-A and Co–O in $La_{0.3}$-5582, as has been explained by HRTEM, EXAFS, and XANES results (Figure 1 and 5, Supporting Information, Figure S8a).[9]

In conclusion, we have shown that catalytic activities of La-doped BSCF5582 ($La_{0.3}$-5582) complex pervoskite catalyst are competitive with the well-known precious metal-based catalysts, RuO_2 and IrO_2, and the formation of rhombohedral $LaCoO_{3-\delta}$ cobaltite particles on the grain surfaces were investigated with HRTEM, XPS, XANES, and EXAFS analyses. The increased number of active sites with increasing surface area is likely to favor both ORR and OER catalysis. However, in the consideration that RuO_2, which is used as a reference material in this study, consists of nanosized particles, circa 50 nm (Supporting Information, Figure S4a), not only the smaller particle size of $La_{0.3}$-5582 at about 1 μm but also the formed $LaCoO_{3-\delta}$ cobaltite nanoparticle are expected to contribute to the enhancement of electrocatalytic performance, for the $LaCoO_{3-\delta}$ cobaltite is a well-known perovskite catalyst for environmental applications.[10] The finding of this novel perovskite catalyst would widen the potential of cheap and bifunctional complex perovskite catalysts into the application, and provide insight into the monitoring of defect chemistry oriented to the enhancement of electrochemical performance in the ceramic-based catalysts.

Received: December 27, 2103
Published online: March 28, 2014

Keywords: electrocatalysts · heterogeneous catalysis · oxygen evolution reaction · oxygen reduction reaction · perovskites

[1] a) F. Cheng, T. Zhang, Y. Zhang, J. Du, X. Han, J. Chen, *Angew. Chem.* **2013**, *125*, 2534–2537; *Angew. Chem. Int. Ed.* **2013**, *52*, 2474–2477; b) Z. Chen, D. Higgins, A. Yu, L. Zhang, J. Zhang, *Energy Environ. Sci.* **2011**, *4*, 3167–3192; c) G. Wu, K. L. More, P. Xu, H.-L. Wang, M. Ferrandon, A. J. Kropf, D. J. Myers, S. Ma, C. M. Johnston, P. Zelenay, *Chem. Commun.* **2013**, *49*, 3291–3293.

[2] a) Y. Matsumoto, H. Yoneyama, H. Tamura, *Bull. Chem. Soc. Jpn.* **1978**, *51*, 1927–1930; b) Y. Matsumoto, H. Yoneyama, H. Tamura, *J. Electroanal. Chem.* **1977**, *79*, 319–326; c) O. Bockris, T. Otagawa, *J. Electrochem. Soc.* **1984**, *131*, 290–302.

 © 2014 Wiley-VCH Verlag GmbH & Co. KGaA, Weinheim

[3] a) J. Suntivich, H. A. Gasteige, N. Yabuuchi, H. Nakanishi, J. B. Goodenough, Y. Shao-Horn, *Nat. Chem.* **2011**, *3*, 546 – 550; b) J. Suntivich, K. J. May, H. A. Gasteiger, J. B. Goodenough, Y. Shao-Horn, *Science* **2011**, *334*, 1383 – 1385; c) A. Grimaud, K. J. May, C. E. Carlton, Y. L. Lee, M. Risch, W. Hong, J. Zhou, Y. Shao-Horn, *Nat. Commun.* **2013**, *4*, 2439 – 2445.

[4] a) Z. Shao, S. M. Halle, *Nature* **2004**, *431*, 170 – 173; b) Z. Shao, W. Yang, Y. Kong, H. Dong, J. Tong, G. Xiong, *J. Membr. Sci.* **2000**, *172*, 177 – 188; c) E. Bucher, A. Egger, P. Ried, W. Sitte, P. Holtappels, *Solid State Ionics* **2008**, *179*, 1032 – 1035; d) J.-I. Jung, D. D. Edwards, *J. Eur. Ceram. Soc.* **2012**, *32*, 3733 – 3743; e) J.-I. Jung, S. T. Misture, D. Edwards, *Solid State Ionics* **2010**, *181*, 1287 – 1293; f) K. Efimov, Q. Xu, A. Feldhoff, *Chem. Mater.* **2010**, *22*, 5866 – 5875; g) M. Lynch, L. Yang, W. Qin, J. J. Choi, M. F. Liu, K. Blinn, M. Liu, *Energy Environ. Sci.* **2011**, *4*, 2249 – 2258; h) G. Kim, S. Wang, A. J. Jacobson, Z. Yuan, W. Donner, C. L. Chen, L. Reimus, P. Brodersen, C. A. Mims, *Appl. Phys. Lett.* **2006**, *88*, 024103; i) J. Liu, G. Collins, M. Liu, C. Chen, J. He, J. Jiang, E. I. Meletis, *Appl. Phys. Lett.* **2012**, *100*, 193903.

[5] a) V. G. Bhide, D. S. Rajoria, G. R. Rao, C. N. R. Rao, *Phys. Rev. B* **1972**, *6*, 1021 – 1032; b) G. Maris, Y. Ren, V. Volotchaev, C. Zobel, T. Lorenz, T. T. M. Palstra, *Phys. Rev. B* **2003**, *67*, 224423; c) S. Uhlenbruck, F. Tietz, *Mater. Sci. Eng. B* **2004**, *107*, 277 – 282; d) G. Thornton, B. C. Tofield, A. W. Hewat, *J. Solid State Chem.* **1986**, *61*, 301 – 307.

[6] G. King, P. M. Woodward, *J. Mater. Chem.* **2010**, *20*, 5785 – 5796.

[7] a) C. A. Randall, A. S. Bhalla, T. R. Shrout, L. E. Cross, *J. Mater. Res.* **1990**, *5*, 829 – 834; b) J. Chen, H. M. Chan, M. P. Harmer, *J. Am. Ceram. Soc.* **1989**, *72*, 593 – 598; c) P. K. Davies, M. A. Akbas, *J. Phys. Chem. Solids* **2000**, *61*, 159 – 166; d) I.-W. Chen, P. LI, Y. Wang, *J. Phys. Chem. Solids* **1996**, *57*, 1525 – 1536; e) L. Farber, P. Davies, *J. Am. Ceram. Soc.* **2003**, *86*, 1861 – 1866.

[8] a) J. B. Goodenough, *Phys. Rev.* **1955**, *100*, 564 – 573; b) Y. Wang, J. Ren, Y. Wang, F. Zhang, X. Liu, Y. Guo, G. Lu, *J. Phys. Chem. C* **2008**, *112*, 15293 – 15298.

[9] a) J. I. Jung, D. D. Edwards, *J. Solid State Chem.* **2011**, *184*, 2238 – 2243; b) J. I. Jung, D. D. Edwards, *J. Mater. Sci.* **2011**, *46*, 7415 – 7422; c) R. P. Vasquez, M. P. Siegal, D. L. Overmyer, Z. F. Ren, J. Y. Lao, J. H. Wang, *Phys. Rev. B* **1999**, *60*, 4309 – 4319; d) N. A. Merino, B. P. Barbero, P. Eloy, L. E. Cadus, *Appl. Surf. Sci.* **2006**, *253*, 1489 – 1493; e) B. Liu, Y. Zhang, L. Tang, *Int. J. Hydrogen Energy* **2009**, *34*, 435 – 439; f) B. K. Kang, H. C. Lee, Y. W. Heo, J. J. Kim, J. Y. Kim, J. H. Kim, *Ceram. Int.* **2013**, *39*, 8267 – 8271.

[10] a) B. Seyfi, M. Baghalha, H. Kazemian, *Chem. Eng. J.* **2009**, *148*, 306 – 311; b) H. Taguchi, S. Yamasaki, A. Itadani, M. Yosinaga, K. Hirota, *Catal. Commun.* **2008**, *9*, 1913 – 1915; c) Y. Zhu, R. Tan, T. Yi, S. Ji, X. Ye, L. Cao, *J. Mater. Sci.* **2000**, *35*, 5415 – 5420.

© 2014 Wiley-VCH Verlag GmbH & Co. KGaA, Weinheim